Exploration of Fiber Fabry-Perot Resonators as Optical Filters

Bachelorarbeit in Physik

von
Fabian König

angefertigt am
Institut für Angewandte Physik,

vorgelegt der
Mathematisch-Naturwissenschaftlichen Fakultät
der
Universität Bonn

Juli 2015

1. Gutachter: Prof. Dr. Dieter Meschede
2. Gutachter: Dr. Wolfgang Alt

Contents

1 Introduction

"Fabry-Perot resonators entered the scene of physics more than a century ago and have continued to play an important role ever since" [1].

Considering the amount of applications of Fabry-Perot resonators nowadays, this statement is unequivocally valid. On the one hand, Fabry-Perot resonators constitute a key component within lasers which are fundamental necessary instruments for current research and industrial processing. On the other hand, Fabry-Perot resonators can provide an intense electromagnetic field confined to a small space, a property which is required for experiments on coupling of single atoms with photons. Not long ago, this rapidly developing field of research – **C**avity **Q**uantum **E**lectro**d**ynamics – started to employ microfabricated fiber-based Fabry-Perot cavities with their desirable small and easily accessible mode volumes. Besides examination of fundamental quantum mechanics, these cavities are promising systems for applications in the aspiring field of quantum information science. Furthermore, fiber-based Fabry-Perot cavities are very qualified for the use as optical filters with narrow bandwidth and high transmission on resonance. Such kind of filter is important for and frequently utilized in a wide variety of applications, for example in telecommunication systems or in spectroscopy experiments.

Two areas of focus of this thesis are the polarization mode splitting and the transmission of a fiber cavity on resonance. A new fiber-based Fabry-Perot cavity which shall subsequently be employed as a filter cavity will be set up.

Polarization mode splitting of the cavity resonances occurs in every optical resonator to a certain extent and is an unwanted effect for many applications of Fabry-Perot cavities. Consequently, it is necessary to be able to control and minimize the mode splitting. A characterization of this phenomenon and the clarification of an earlier measurement on the subject are the topic of chapter 3.

One essential figure of merit of an optical filter is a high transmission on resonance. Considering fiber-based Fabry-Perot resonators, the amount of transmitted power is very sensitive on the alignment and geometry of the fibers. Chapter 4 is devoted to a theoretical and experimental discussion of how to optimize a fiber cavity for high transmission.

In order to provide the theoretical basics, the principle behind a Fabry-Perot resonator and its fundamental mode are recapitulated and general information about fabrication and properties of fiber resonators are presented in chapter 2.

2 Theory of Fabry-Perot Resonators

In 1897, Charles Fabry and Alfred Perot utilized multiple-beam-interference between two planar mirrors in order to construct an interferometer. Nowadays, modern physics can not be imagined without "Fabry-Perot Resonators". The following chapter presents an outline of the functionality principle behind this kind of resonator.

2.1 Functionality

The easiest way to build up a Fabry-Perot resonator is to arrange two planar mirrors opposed to each other, forcing light to bounce back and forth and thus, to interfere with itself. Monochromatic polarized light of frequency ν and wavevector $\vec{k}$ is given as a solution of Maxwell's equations by a plane wave with the complex wavefunction

$$\vec{E}(\vec{x},t) = \vec{E}_0 \ \exp\left(i(\vec{k}\vec{x} - 2\pi\nu t + \varphi)\right) \qquad k := \left|\vec{k}\right| = \frac{2\pi}{\lambda} = \frac{2\pi}{c}\nu \tag{2.1}$$

where c denotes speed of light in the surrounding medium (usually air). Because light inside the resonator will interfere with itself, only beams of certain wavelengths will interfere constructively, so called "modes". These modes which will form standing waves can be determined by considering that they reproduce themselves after a single round-trip. Since the additional phase shift on each mirror is π (which imparts 2π after one round-trip), the physical relevant phase shift $\Delta\varphi$ after one round trip is only defined by the distance L of the two mirrors. Claiming this phase shift to be a multiple of 2π, one obtains

$$\Delta\varphi = k \cdot 2L = \frac{2\pi}{c}\nu \cdot 2L \stackrel{!}{=} q \cdot 2\pi \qquad q \in \mathbb{N}_{>0} \tag{2.2}$$

$$\implies \nu_q = q \cdot \frac{c}{2L} \tag{2.3}$$

the resonance frequencies ν_q of the resonator with given length L. These adjacent frequencies are spaced by the *Free-Spectral-Range* FSR

$$\mathrm{FSR} = \nu_q - \nu_{q-1} = \frac{c}{2L}. \tag{2.4}$$

One would alternatively obtain the resonance frequencies by considering the transverse component of the electric field to vanish at the mirrors, which is a natural boundary condition on (perfect) electrically conducting materials.

The strict condition of single resonance frequencies allowed to propagate inside the cavity is relaxed considering real mirrors. In reality a mirror is not perfect, which is characterized by its power reflection and transmission R and T, respectively, or analogously by its effect on the complex wavefunction expressed by the amplitude attenuation factors $r, t \in \mathbb{C}$ with $|t|^2 = T$, $|r|^2 = R$. Moreover, losses L can occur because of absorption or scattering, for instance. The relation $R + T + L = 1$ is valid due to energy conservation. As a con-

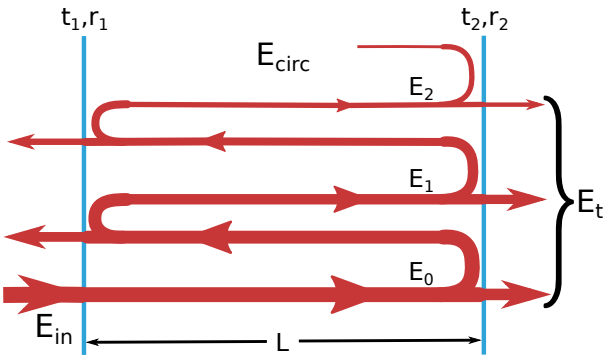

Fig. 2.1: Multiple reflections and transmissions of light inside a cavity. The intensity of each field is given by $I = |E|^2$.

sequence, not only optical waves with discrete frequencies, but a continuous **spectrum** appears inside the cavity. Imagine the light beam on its way through the resonator as depicted in fig. 2.1. An incident light wave E_{in} (polarization is neglected here) with intensity $I_{in} = |E_{in}|^2$ passes the first mirror and a fraction $E_0 = t_1 E_{in}$ is transmitted into the cavity. Here, it undergoes multiple transmissions and reflections, so that the overall field E_{circ} circulating inside the cavity can be expressed as the sum of the infinite internal light waves which are continuously reflected. By taking the additional phase shift $\Delta\varphi$ after one-round trip into account, E_{circ} is given by

$$\left.\begin{aligned} E_0 &= t_1 \cdot E_{in} \\ E_1 &= r_1\, r_2\, \mathrm{e}^{-i\Delta\varphi} \cdot E_0 \\ E_2 &= r_1^2\, r_2^2\, \mathrm{e}^{-2i\Delta\varphi} \cdot E_0 \\ E_3 &= r_1^3\, r_2^3\, \mathrm{e}^{-3i\Delta\varphi} \cdot E_0 \\ &\vdots \end{aligned}\right\} \quad E_{circ} = \sum_i E_i = E_{in}\, \frac{t_1}{1 - r_1 r_2 \mathrm{e}^{-i\Delta\varphi}} \tag{2.5}$$

Using equations (2.2), (2.4) and the geometric series, an intensity distribution inside the cavity can be determined as

$$I_{circ}(\nu) = |E_{circ}|^2 = \frac{I_{max}}{1 + \left(\frac{2\mathscr{F}}{\pi}\right)^2 \sin^2\left(\frac{\pi\nu}{\mathrm{FSR}}\right)} \tag{2.6}$$

$$I_{max} = I_{in}\frac{T_1}{(1-\sqrt{R_1 R_2})^2}, \qquad \mathscr{F} = \frac{\pi \sqrt[4]{R_1 R_2}}{1 - \sqrt{R_1 R_2}} \tag{2.7}$$

and the normalized transmission spectrum reads

$$T(\nu) = \frac{I_t}{I_{in}} = \frac{|t_2 \cdot E_{circ}|^2}{I_{in}} = \frac{T_{max}}{1 + \left(\frac{2\mathscr{F}}{\pi}\right)^2 \sin^2\left(\frac{\pi\nu}{\mathrm{FSR}}\right)}, \qquad T_{max} = \frac{T_1 T_2}{(1-\sqrt{R_1 R_2})^2} \tag{2.8}$$

These are periodic functions of frequency, see fig. 2.2. The resonator behaves completely transparent on resonance for $T_1 = T_2$ and in case of no absorption losses ($R_i = 1 - T_i$), otherwise $T_{max} < 1$. The **finesse** $\mathscr{F}$ is proportional to the lifetime of a photon inside the cavity. If it is large, $\mathscr{F} \gg 1$, the intensity is sharply peaked around the resonance frequencies and the intensity I_{max} of the intra-cavity field on resonance can be enormously higher than the incident intensity. The full-width-at-half-maximum FWHM is then given by $\mathrm{FWHM} = \mathrm{FSR}/\mathscr{F}$, which means for large $\mathscr{F}$ the resonance peaks are quite narrow compared to the FSR. This is one main reason for employing Fabry-Perot resonators as optical filters. They can be tuned by adjusting the length of the cavity. For macroscopic cavities ($L \approx 1\,\mathrm{cm}$) however, the resonance frequencies are very sensitive to small changes ΔL of the cavity length, since $\Delta\nu_q = q\mathrm{FSR}\Delta L/L$. As an example, for typical frequencies of $\nu_q \approx 5\,\mathrm{THz}$, the order is $q \approx 17\,000$, so that even a small change in cavity length $\Delta L/L = 10^{-3}$ alters the resonance frequencies by $\Delta\nu_q \approx 250\,\mathrm{GHz}$. The change of the free spectral range is only $\Delta\mathrm{FSR} \approx 15\,\mathrm{MHz}$.

All things considered, a high finesse is desirable in order to obtain a Fabry-Perot filter cavity with sharp transmission peaks permitting only a small band of selected frequencies to be transmitted. Of course, losses on the mirror surfaces should be reduced in order to transmit as much power as possible on resonance.

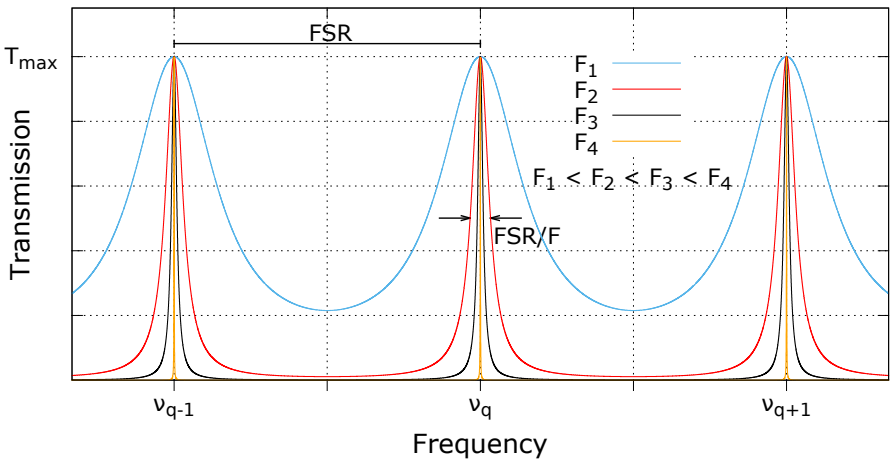

Fig. 2.2: The transmission spectrum for different values of the finesse is a function with periodicity FSR. If $\mathscr{F} \gg 1$, the peaks are approximately described by Lorentz-peaks.

Ray confinement – geometric stability

One disadvantage of two parallel planar-mirrors with finite diameter is the high sensitivity on misalignment. If the to mirrors are not perfectly parallel, rays will leak out of the resonator after some round-trips. Other cavity geometries providing a more stable ray confinement are possible. A quantity to characterize this stability is given by the *g-parameters* of the two mirrors with radii of curvature R_1, R_2 and distance L (concave mirrors have $R = -|R|$). A stable resonator must provide

$$0 \leq g_1 \cdot g_2 \leq 1, \qquad g_i = 1 + \frac{L}{R_i} \tag{2.9}$$

which is graphically presented in fig. 2.3. A detailed derivation can be found in [3].

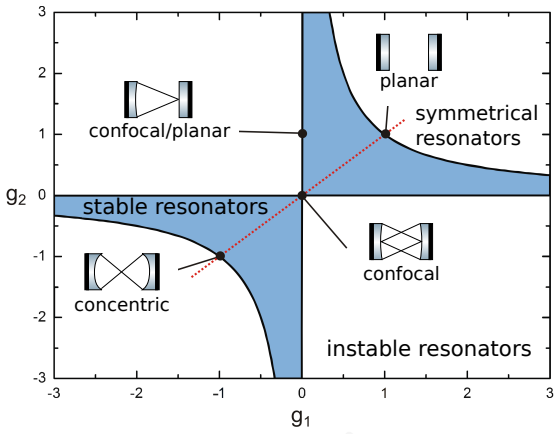

Fig. 2.3: Stability diagram. The blue area marks the regime of stable resonators, symmetric resonators with $R_1 = R_2$ lie on the red dashed line. Some special examples are given. Parts of the image are taken from [2].

2.2 The Gaussian Beam

So far, the description of light inside a cavity via a plane wave was sufficient. However, a plane wave is not spatially confined and can not provide any information about the spatial distribution of the intensity. Considering a special case of Maxwell's equations, the paraxial Helmholtz-equation, one can find the *Hermite-Gaussian-Beams* as a whole set of orthonormal solutions. These do provide information about a spatial intensity distribution. The lowest order solution – the so called **Gaussian Beam** – is of most importance as it describes laser beams and modes inside a cavity to good approximation. In the following, only a brief outline of the most important properties of the Gaussian beam shall be outlined, since good and far more detailed treatments of the quantities and their relationships can be studied in textbooks like [3].

Let z be the propagation axis and $\rho = x^2 + y^2$ the radial distance from any point to this axis. The intensity of a Gaussian beam in any transverse plain is concentrated

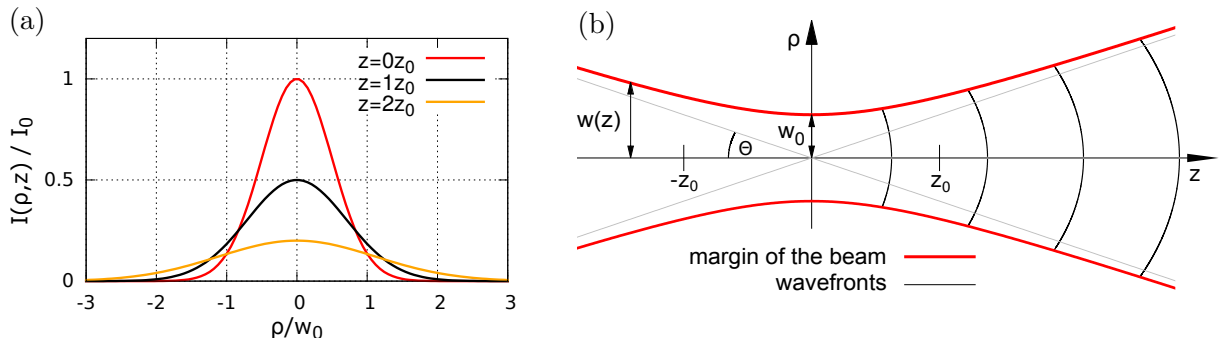

Fig. 2.4: (a) Radial intensity profile. For $z = z_0$, the intensity on the axis is halved. (b) The radius obtains its minimum value at the beam waist and increases linearly with z for large z. The wavefront normals are paraxial rays. Sketch (b) partly from [4].

and distributed spherically symmetric around the propagation axis, following a Gauss-function (see fig. 2.4a). The width $w(z)$ of this Gauss function is defined as the radial distance where the intensity drops to $1/e^2$ of the peak intensity. w is known as the radius of the beam at position z. This radius takes its minimum value w_0 at the beam's waist and grows successively in both directions, which means the beam is converging left and diverging right of its waist as illustrated in fig. 2.4b. Moreover, after a "Rayleigh range" z_0 from the waist the intensity on the z-axis drops to half its value.

The Gaussian beam is of interest in the context of this thesis because it is a good approximation for a beam exiting single mode fibers which are frequently used in the experiments, and because it describes a mode inside a fiber cavity.

Gaussian mode inside a cavity

Imagine two mirrors left and right of the beam's waist opposing each other. If the radius of curvature of the beam's wavefronts at the positions of the mirrors is identical to the mirror radii, the Gaussian beam will retrace itself after one round trip and thus forms a self consistent mode (a treatment of the phase is neglected here).

Because a mathematical description is essential for a discussion of mode-matching efficiencies of Gaussian beams, which is the topic of chapter 4, we now specify a Gaussian beam matching a resonator. Let R_i be the radius of curvature of the mirror located at position z_i (the beam waist w_0 be at $z = 0$). Since both mirrors are separated by a distance L, $z_2 = z_1 + L$ is valid. Considering the condition that the wavefront curvature at the mirrors is identical with the mirror curvatures, one obtains [3]

$$z_1 = \frac{-L(R_2 + L)}{R_1 + R_2 + 2L}, \qquad z_2 = z_1 + L \tag{2.10}$$

$$z_0 = \frac{-L(R_1 + L)(R_2 + L)(R_1 + R_2 + L)}{(R_1 + R_2 + 2L)^2} \tag{2.11}$$

for mirror positions and Rayleigh range ($R_i < 0$ for concave mirrors). These parameters completely describe the mode. Important parameters are the beam radii w_0 at the waist and $w_{m,i}$ at the mirror $i = 1, 2$, given by

$$w_0 = \sqrt{\frac{\lambda z_0}{\pi}}, \qquad w_{m,i} = w_0 \sqrt{1 + \left(\frac{z_i}{z_0}\right)^2}. \tag{2.12}$$

For mirror radii between 140 µm to 210 µm and cavity lengths between 10 µm to 50 µm,

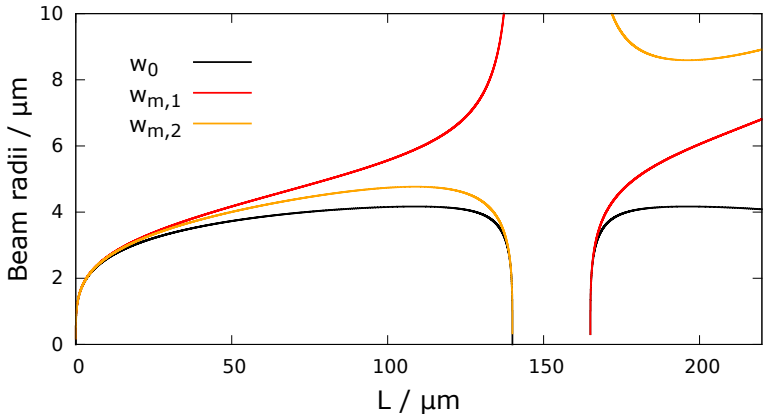

Fig. 2.5: Beam radii $w_{m,1}, w_{m,2}$ at the mirrors and minimum beam radius w_0 at the waist versus the length of the cavity L for two mirrors with radii of curvature $R_1 = 140\,\mu\text{m}$, $R_2 = 165\,\mu\text{m}$ and light at 780 nm wavelength. For small mirror distances the radii are almost constant, which implies that the Rayleigh range is much larger than L. The singularities around 140 µm originate from a violation of the geometric stability condition (2.9).

which are reasonable values for fiber cavities, the beam is focused down to only 2 µm to 4 µm at both, waist and mirrors (see fig. 2.5). Moreover, the divergence is really small, which is due to a large Rayleigh range between 40 µm to 60 µm for this set of parameters.

The resonance frequencies of a Gaussian beam inside a cavity are identical to those of a plane wave, but only shifted by a constant displacement This especially means that the free spectral range stays the same. Why is it legitimate to state that the Gaussian beam is the dominant mode inside a fiber cavity? A beam exiting a singlemode fiber is well approximated by a Gaussian beam, and entering the cavity, it is projected on an orthonormal set of all possible cavity modes. Due to the similarity of the mode field radii of the Gaussian beam exiting the fiber and of the Gaussian beam inside the cavity, the overlap of both is quite large compared to the overlaps with other cavity modes (see also chapter 4). Consequently, the Gaussian beam is the dominating intra-cavity mode.

2.3 Fiber-based Fabry-Perot cavities

Fiber-based Fabry-Perot cavities offer numerous advantages for CQED experiments. They combine small and easily accessible mode volumes with a potentially high finesse. Moreover, there is no need of further mode-matching optics which make them very applicable for the assembly in integrated systems. Fiber resonators consist of two optical glass fibers arranged opposite to each other, as shown in fig. 2.6. The fiber tips are microfabricated mirrors, thus, the setup is in principle a normal Fabry-Perot resonator. What makes it so interesting for current research is the possibility that the the mirrors can approach each other up to $L \approx 8\,\mu\text{m}$ (only a few $\lambda/2$ and shorter than the Rayleigh range) due to their tiny diameter, resulting in very small and almost constant waists inside the cavities between typical values of 2 µm to 4 µm. The corresponding small mode volumes are highly desirable for light-matter-interaction experiments.

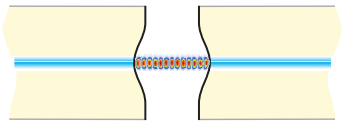

Fig. 2.6: Sketch of the geometry of an aligned fiber-based cavity. Taken from [5].

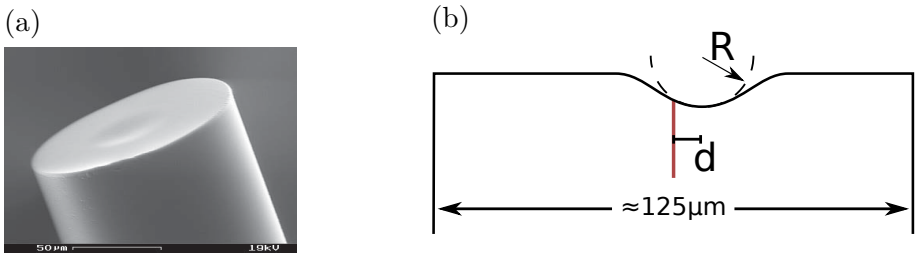

Fig. 2.7: (a) Scanning electron microscope image of a fabricated fiber tip. Taken from [5]. (b) Cross section of a mirror-fiber. The concave depression can be approximated to first order by a sphere of radius R. Moreover, a decentration d can be recognized (the red line represents the fiber core). Typical single-mode fibers have a cladding diameter of $\approx 125\,\mu m$.

Fabrication and Characterization

The current optimal way to fabricate the required fibers is to focus a CO_2 laser pulse onto a cleaved fiber tip [6]. It evaporates the fiber by heating it up, resulting in a concave shape with very low surface roughness which minimizes scatter losses (see fig. 2.7a). In a next step, a high reflective coating is deposed onto the fiber end faces.

In order to characterize the mirrors in terms of the radius of curvature, an interferometric microscope is employed allowing to fit a sphere to the mirror cross-sections. Thus, the radius of curvature R can be determined. However, two very important figures of merit have to be considered here, of which the first one is **ellipticity**. In general, the mirror surfaces are not perfect spherical but exhibit ellipticity, that is, their surface near the centre can be approximated by an elliptical paraboloid with a mayor axis of radius of curvature R_1 and a perpendicular minor axis with radius of curvature R_2 [1]. This leads to important phenomena which are examined in chapter 3.

The second significant cavity mirror parameter is **decentration**, which occurs if the CO_2-beam has not been perfectly centered on the fiber core. The distance d of the centre of the concave profile to the fiber core is called decentration, as depicted in fig. 2.7b. This effects the coupling of the fiber mode with the cavity mode, which is treated in more detail in chapter 4.

Properties of the employed fibers

A short outline of the fibers used in this thesis shall be given here. All the fibers, of which the most are singlemode and few are multimode fibers, have identical coatings. The singlemode fibers *CU800* are ordered from the company IVG Fiber and have a measured mode field diameter of $(4.8 \pm 0.2)\,\mu m$, a cladding diameter of $(125 \pm 1)\,\mu m$ and a cut-off wavelength of 770 nm. The dielectric coatings are optimized for 780 nm. For light at 850 nm wavelength, which is used in the experiments of this thesis as well, the transmission T is higher resulting in a decreased finesse. Table 2.1 presents T and L values of the coatings, as well as theoretical finesses to expect. The equations (2.7) and (2.8) for the finesse and the maximal achievable transmission can be approximated for low T and L using the taylor expansion:

$$\mathscr{F} \approx \frac{2\pi}{T_1 + T_2 + L_1 + L_2}, \qquad T_{max} \approx \frac{4T_1T_2}{(T_1 + T_2 + L_1 + L_2)^2} \tag{2.13}$$

Typical radii of curvature are 140 µm to 210 µm, most fibers exhibit decentrations in a range from 0.5 µm to 4 µm. Ellipticity can mainly be found in a range from R_1/R_2=1.02 to 1.13.

	780 nm	850 nm
T/ppm	13 ± 3	134 ± 4
L/ppm	13 ± 3	13 ± 3
$\mathscr{F}$	$121\,000 \pm 14\,000$	$21\,400 \pm 500$
T_{max}/%	25 ± 6	83 ± 3
γ / dB	48.9 ± 0.5	41.3 ± 0.1

Tab. 2.1: Properties of the coatings of our fibers. Finesse and T_{max} are calculated via eq. (2.13), extinction γ via eq. (2.14).

2.4 Filter cavities

Optical filters are an important technology with applications in telecommunications, in setups where they separate laserfields with small frequency spacings, or in current modern atomic physics experiments, just to mention a few. Because Fabry-Perot cavities only transmit light around distinct resonance frequencies and reflect all other frequencies, they can be employed as excellent optical filters. However, the spectrum of source light should be smaller than the free spectral range in order to avoid ambiguity. If the finesse is high, the transmitted bandwidth is small and the extinction ratio, that is the ratio between the intensity of the transmitted light on and off resonance, is large. All things considered, important figures of merit of an optical Fabry-Perot filter are:

- High transmission on resonance
- Narrow bandwidth FWHM
- Large extinction ratio
- Large free spectral range FSR

The transmission on resonance is very sensitive on the coating parameters as can be seen in equation (2.8). Moreover, it depends on the coupling of the fiber mode with the cavity mode, which is sensitive on the alignment and the geometry of the fiber mirrors. All other quantities mentioned above are related to the optical finesse. Comparing the transmitted intensity on resonance $I_t(\nu_q)$ with the transmitted intensity off resonance $I_t(\nu = \nu_q + \frac{\mathrm{FSR}}{2})$, the extinction ratio reads:

$$\gamma(\mathscr{F}) \coloneqq \frac{I_{on}}{I_{off}} = 1 + \frac{2\mathscr{F}}{\pi} \tag{2.14}$$

Consequently, a high finesse yields a large extinction. Furthermore, since $\mathscr{F} = {}^{\mathrm{FSR}}/_{\mathrm{FWHM}}$, a large FSR and a narrow bandwidth are complementary quantities for a given finesse. That is why a high finesse is desirable to obtain a large FSR and a small FWHM simultaneously. However, in the case of significant losses in the mirror coatings, one is confronted with a trade-off between large finesse, which requires low transmission of the mirror coatings, and large transmission on resonance, which requires high coating transmissions. This trade-off and the coupling of the fiber and cavity modes is topic of chapter 4.

All in all, fiber-based Fabry-Perot cavities are very qualified for the employment as optical filters with excellent properties. The finesse is very high and due to the small mirror distance the FSR is very large. Thus, it is possible to transmit light in a small frequency range and to simultaneously extinguish all other effectively. For example, choosing a typical fiber-cavity length of 25 µm and a finesse of 100 000, the free spectral range is ≈ 6 THz. The linewidth of the transmission peaks is around 60 MHz, that means it is five orders of magnitude smaller!

2.5 The "SM-MM cavity"

For the work on this thesis a new fiber-based cavity was set up. When choosing the fibers, one main aspect was taken into account: The fibers should provide a large polarization mode splitting in order to grant the possibility of examining this effect in more detail, which is the topic of chapter 3. Therefore, the fibers must provide a large ellipticity [1]. Furthermore, the new cavity shall serve as an optical filter cavity, which led to the decision for a combination of a singlemode (SM) input and a multimode (MM) output fiber. That is because a multimode fiber with its large numerical aperture gathers more light from the intra-cavity field resulting in a maximum filter transmission (see chapter 4 on mode-matching efficiency for details).

Table 2.2 presents the properties of the chosen fibers. While the cavity length is scanned over two adjacent resonances, the free spectral range and the linewidth of the transmission and reflection peaks can be measured via an oscilloscope, yielding a finesse of

$$\begin{aligned} \lambda = 850\,\mathrm{nm} \quad &\Longrightarrow \quad \mathscr{F} = 24\,300 \pm 300 \\ \lambda = 780\,\mathrm{nm} \quad &\Longrightarrow \quad \mathscr{F} = 189\,000 \pm 8000 \end{aligned}$$

which is quite large compared to the theoretical values in table 2.1. The accuracy of this kind of finesse measurement is discussed in appendix A. A summary of the measured figures of merit for this particular cavity can be found in the concluding chapter 5.

Whenever in the following text it says "the SM-MM setup" or "the SM-MM cavity", this cavity is meant.

	SM fiber	MM fiber
Major ellipticity axis R_1	$(165 \pm 10)\,\mu\mathrm{m}$	$(191 \pm 10)\,\mu\mathrm{m}$
Minor ellipticity axis R_2	$(139 \pm 10)\,\mu\mathrm{m}$	$(167 \pm 10)\,\mu\mathrm{m}$
Ellipticity R_1/R_2	1.19 ± 0.11	1.14 ± 0.09
Decentration d	$(1.82 \pm 0.25)\,\mu\mathrm{m}$	$(3.82 \pm 0.25)\,\mu\mathrm{m}$

Tab. 2.2: Properties of the fiber mirrors of the SM-MM cavity. Both mirrors exhibit a large ellipticity, which should lead to a distinct polarization mode splitting. The very large decentration of the MM fiber does not have major effects, since a MM fiber gathers almost all the intra-cavity light anyway.
The radii of curvature (ROC) of the two ellipticity axes are determined by fitting a sphere to 30 µm of the mirror cross sections. Fits to 20 µm or 40 µm of the surface yield the deviation of the ROC around 10 µm. The decentration of the fiber core is measured by illuminating it from the back and imaging it with a microscope. The error 0.25 µm is dominated by the microscope resolution.

3 Polarization mode splitting

3.1 Origin

In experiments with fiber-based Fabry-Perot cavities a mode splitting of two slightly different resonance frequencies can be observed. This originates from two sources. The first one is birefringence, as stress on the microscopic fiber mirrors induces slightly different optical path lengths for two different axes. Polarized light will thus be separated into two non-degenerate eigenmodes. The second is ellipticity of the mirrors due to production issues, leading to two perpendicular axes. It has been shown in [1] that corrections to the scalar paraxial resonator theory by extending it to a vector theory and including polarization agree excellently with experimental results. Geometry of the mirror surfaces is found to be the dominant source of polarization mode splitting in microscopic cavities.

Since controlling polarization mode splitting is essential to obtain one instead of two slightly different resonance frequencies, which is important for a filtering of narrow bandwidths, this chapter is devoted to a characterization of this phenomenon.

The setup used for the investigation is shown in fig. 3.1. The fibers are situated on three-dimension translation stages, one of which is equipped with a piezo crystal connected to a frequency generator so that the cavity length can be scanned. Linear polarized light exiting the isolator enters the fiber. Assuming the fiber to guide the light independently of its polarization and to not further affect it (which is a tolerant simplification and considered in more detail in section 3.3), linear polarized light will also emerge inside the cavity.

The $\lambda/2$ retardation waveplate is a key component in the setup. This kind of waveplate rotates incoming linear polarized light about an angle 2θ, which is twice as big as the angle θ of the waveplate's extraordinary axis with respect to the incident polarization. Consequently, if $\theta = 90°$, linear polarized light is mapped on itself despite a physically non-relevant and non-observable additional phase shift of π. By rotating this waveplate, the linear polarization vector of the light inside the cavity is rotated as well. In steps of

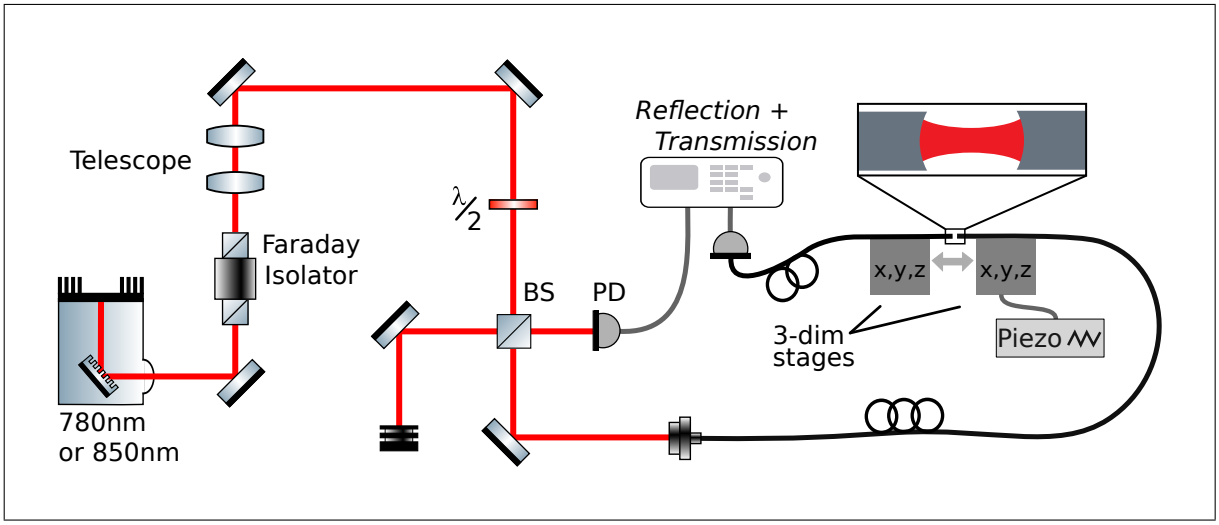

Fig. 3.1: Principal setup used to investigate polarization mode splitting. The key-component is a $\lambda/2$ retardation waveplate as explained in the text. With photodiodes (PD), the reflection and transmission signals are recorded on an oscilloscope. BS=Beamsplitter.

$\theta = 45°$ it can be chosen parallel to one of the two perpendicular ellipticity axes, namely *fast* and *slow* axis. Thus, the cavity modes corresponding to the two ellipticity axes can be populated separately and only one resonance frequency remains. In between, both axes are populated simultaneously and two slightly different resonance frequencies occur (see fig. 3.2). All things considered, by rotating the waveplate a periodicity of 90° is expected.

In the experiments, the cavity resonance lineshapes are recorded as a function of the waveplate's rotation angle. The amplitudes of the two peaks yield information about the population of the two polarization modes, that means, about the intensity distribution in the two ellipticity axes. By recording and fitting more than 15 lineshapes for each rotation angle of the waveplate, the amplitudes of the two peaks are determined by the mean and the error by the standard deviation.

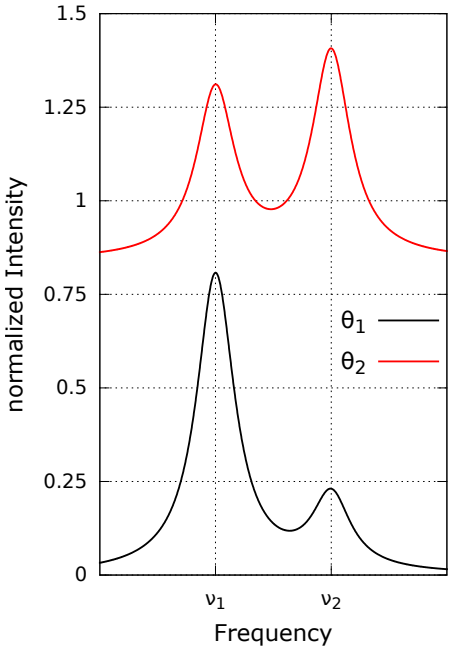

Fig. 3.2: Population of both polarization modes for two different waveplate angles θ. Each mode can be fully populated while the other is depopulated. Output of oscilloscope looks identically but with time on x-axis.

3.2 Measurements

Earlier measurements

A rotation of the $\lambda/2$ retardation waveplate should result in a 90° periodicity of the population of the polarization modes, as pointed out above. In a measurement taken on 15$^{\text{th}}$ April 2014 in this research group, a rotation of the $\lambda/2$ waveplate yielded a periodicity of $\theta = 180°$ which has not been understood and which had been a reason for the following examination.

Resolving mode splitting

The goal of this project was to characterize the polarization mode splitting of the SM-MM cavity and finding an explanation for the so far non-understood periodicity measurement. Therefore, it should be repeated and examined in more detail[1].

Finding and resolving polarization mode splitting appeared to be very challenging at first. Using the SM-MM cavity with laserlight at 850 nm, finesse is measured to be $\mathscr{F} = 24\,300 \pm 300$ and the resonance linewidth[2] is (183 ± 4) MHz for a cavity length of (30 ± 3) µm. But no splitting is observable. This implies two possible conclusions. Either the cavity does not feature a significant mode splitting, which is not very probable since the fibers exhibit large ellipticity, or the spacing of the polarization modes is smaller than the resonance linewidth of around 180 MHz. In this case, the two resonance peaks overlap and are not or almost not separately resolvable and add up to only one "overall" peak. However, it should be possible to see deviations of the lineshape of the resulting peak by rotating the $\lambda/2$ waveplate – if only one polarization mode is populated, the linewidth is smaller than if both modes are populated (the sum of two close adjacent peaks is one peak with larger linewidth than the linewidth of the single peaks). The problem one

[1] See appendix B for photos of the employed alignment stages and of the opposed fibers.
[2] Details about the measurement of the linewidth in units of frequency will follow.

is confronted with at this point is the mechanical jitter of the piezo movement. The permanent small changes in cavity length are reasons why very closely neighboured peaks cannot be resolved and analysed properly.

So, an already existing rigid cavity where strong splitting had already been observed has been employed. This rigid cavity is built by two singlemode fibers glued with their mirror tips into a glass ferrule. Thus, the cavity length is fixed and in order to see a resonance the laser frequency has to be scanned. With laserlight at 850 nm wavelength a slight mode splitting is observable, but not significant enough for an analysis. With laserlight at 780 nm wavelength, other challenges occurred. The employed laser showed a lot of mode jumps making it hardly possible to set it to the right resonance frequency. Another more stable laser diode was then used, but no resonance could be found here as well, since its linewidth around 40 GHz was really narrow, considering a free spectral range of the cavity of around 2.8 THz.

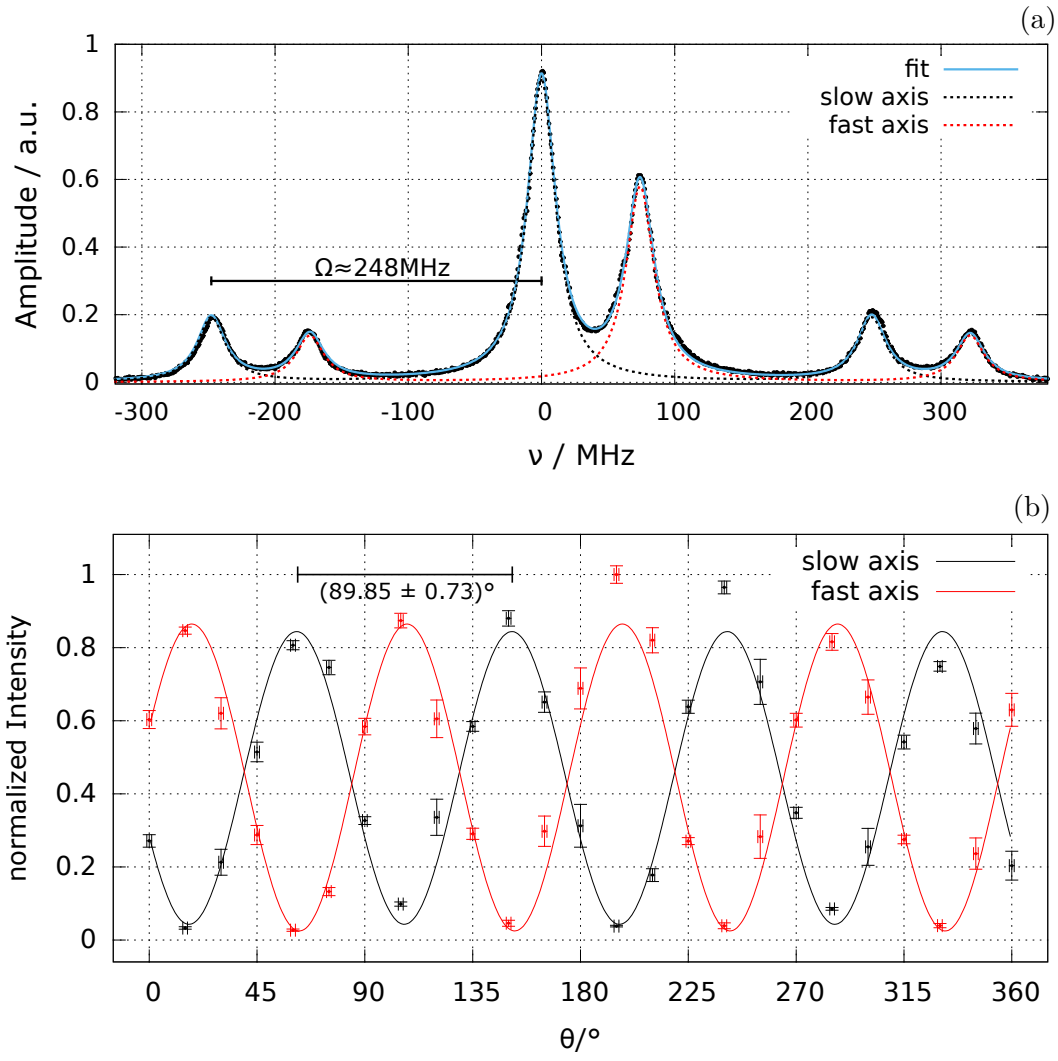

Fig. 3.3: (a) A large splitting between two polarization modes of (3.22 ± 0.10) linewidths is observable. The linewidth of the cavity is (23 ± 1) MHz. The sidebands of an EOM are located symmetrically with identical distance beside each mode and can nicely be distinguished: Sidebands with larger amplitude (black fit) belong to the more populated, sidebands with smaller amplitude (red) to the less populated polarization mode. (b) The amplitudes of both polarization modes versus the angle of the waveplate. The expected periodicity $\approx 90°$ is observed.

Going back to the SM-MM cavity and using a laser at 780 nm wavelength, strong polarization mode splitting could be observed. To obtain the cavity linewidth in units of frequency, an electro-optic modulator (EOM) was used to generate sidebands to the actual transmission peaks with a frequency spacing of $\Omega \approx 248\,\mathrm{MHz}$. Using the sidebands as markers with known frequency displacements it is possible to perform a calibration from time to frequency. This is depicted in fig. 3.3a. Finesse turns out to be $189\,000 \pm 8000$ which is really high compared to theoretical predictions. A narrow linewidth of $(23 \pm 1)\,\mathrm{MHz}$ and a large polarization mode splitting of (3.22 ± 0.10) linewidths can be observed providing great opportunities for the investigation of the behaviour of mode splitting in more detail: The $\lambda/2$ retardation waveplate was rotated one full circle in steps of 15° and for each angle 15 measurements of the Lorentzian amplitudes of both peaks have been recorded. The presented result in fig. 3.3b shows nearly perfect 90° periodicity, matching the expectation.

Up to this point the predictions have been fully confirmed, nevertheless the question about the earlier measurements with 180° periodicity remains. One key discovery was made after some time: It turned out that the waveplate employed in the non-understood measurement one year ago was by mistake a $\lambda/4$- rather than an $\lambda/2$-waveplate (however, the measurement in fig. 3.3b has been realized with the correct waveplate). In order to examine the change in behaviour of the population of slow and fast axis when a $\lambda/4$ retardation waveplate is rotated, the $\lambda/2$-plate was replaced by a $\lambda/4$-plate in the SM-MM setup with 780 nm. Indeed, a new measurement presented in fig. 3.4 yields a periodicity of $(178.36 \pm 1.55)°$. The origin of the earlier non-understood measurement seems to be detected.

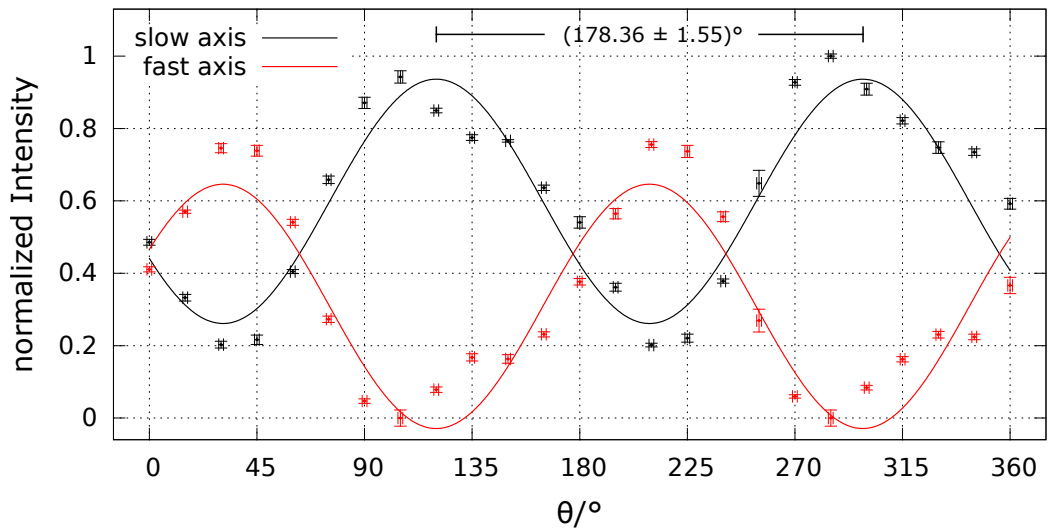

Fig. 3.4: Periodicity measurement with a $\lambda/4$ waveplate. It yields a periodicity of around 180°. However, a sinusoidal fit is not satisfactory.

3.3 Simulation of two combined retardation waveplates

However, around 135° and 315° a significant deviation from the sinusoidal fit in fig. 3.4 occurs. To understand this, one has to consider a $\lambda/4$-waveplate transforming linear polarized into elliptical polarized light. Furthermore, assuming the fiber to have no further effects on the polarization state of the incident light is not sufficient. Indeed, it can transform the polarization state into any other polarization state. Taking this into account, it is hardly imaginable how the outcome of light will look like after having passed the waveplate and the fiber. A simulation shall clarify things.

The simulation utilizes the fact that any polarization state can be written in an orthonormal linear basis including a phase shift between both basis states. If the ordinary and extraordinary axes of a λ/x-waveplate are chosen as basis and a corresponding additional phase shift $\phi = 2\pi/x$ to the one basis state parallel to the extraordinary axis is introduced, the effect of the waveplate can be calculated. In fig. 3.5 the principal idea behind the simulation is presented: Perfect linear polarized incident light in y-direction in front of the first waveplate, which can either be a $\lambda/2$- or $\lambda/4$-plate, is assumed. Having passed it, the light is given in another polarization state. The effect of the fiber on incident polarization states in its most general form requires three parameters (considering the Poincaré-sphere, two parameters define the position of a rotation axis about which any polarization state is rotated and one parameter defines the rotation angle, that is the retardation. See [7] for further information). However, here we make the simplification of simulating the effect of the fiber by assuming it acts as an arbitrary waveplate which is determined by only two parameters, its retardation ϕ_2 and the angle θ_2 of its extraordinary axis with respect to the x-axis[3]. In the end, after going through the fiber, the polarization will be mapped onto a cavity coordinate system defined by the angle θ_C. That offers the chance to find a coordinate system matching the ellipticity axes of the cavity. The result of the simulation is the intensity distribution in both cavity coordinate axes as a function of the angle θ_1 of the first waveplate. This corresponds to the measurements above.

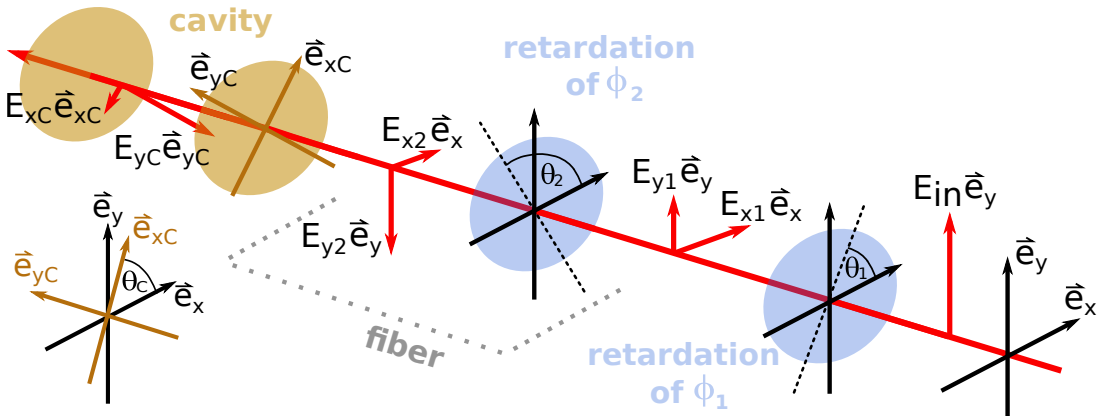

Fig. 3.5: Scheme of the combined-waveplate simulation. Linear polarized light in y-direction passes the first waveplate, which can either be a $\lambda/2$- or $\lambda/4$-plate. The fiber is assumed to act as an arbitrary waveplate with retardation ϕ_2. The final polarization state is mapped onto a cavity coordinate system and the result of the simulation is the intensity in both cavity coordinate axes as a function of the angle θ_1 of the first waveplate.

[3]Because we consider the fiber as an additional waveplate, "fiber" and "second waveplate" are used interchangeably in the following.

Results

The simulation gives two major insights: Using a $\lambda/2$ waveplate, one will always obtain a 90° periodicity independent of the behaviour of the fiber. The only effect the fiber can have is to transform the incident linear into elliptical polarized light which leads to a constant non-vanishing portion of light in both cavity axes. Of course, since the cavity coordinate system is orthogonal, the overall intensity is just the sum of the intensities in each axis.

When using a $\lambda/4$-plate one will obtain a 180° periodicity in general. A special case occurs if the ordinary and extraordinary axes of the second waveplate are chosen parallel to the cavity coordinate axes: Let us assume a $\lambda/4$-plate as first waveplate. A rotation of it leads to a transformation of the incident linear polarized light in y-direction in steps of $\theta_1 = 0°, 45°, 90°...$ from linear polarized light in y-direction into right-circular polarized light, linear polarized light in y-direction, left-circular polarized light and again linear polarized light in y-direction. Both circular polarization states are identical in terms of the intensity distribution per coordinate axis ($1/\sqrt{2}I_0$ in each axis). The linear polarization states into which the light is transformed are also identical in this regard (I_0 in the y-axis and no intensity in the x-axis). So far, the intensity distribution in the x-y-coordinate system shows a 90° periodicity of the rotation of the $\lambda/4$ waveplate. When the polarization states undergo the second waveplate, they will obtain an additional phase shift. However, if the ordinary and extraordinary axes of the second waveplate are parallel to the cavity coordinate system, this additional phase shift has no further effect on the intensity distribution in the cavity coordinate system. Thus, the intensity distribution in the cavity coordinate system shows a 90° periodicity of the rotation of the $\lambda/4$ waveplate, as depicted in fig. 3.6a.

In any other constellation of the simulation parameters one gets results which deviate from a sinus and feature a 180° periodicity. And indeed, it is possible to fit the measurement in fig. 3.4, which is shown in fig. 3.6b. This implies, that the assumption of the fiber acting as a waveplate is sufficient. All things considered, the origin of the measurement results from last year are understood. They resulted from the use of an incorrect waveplate.

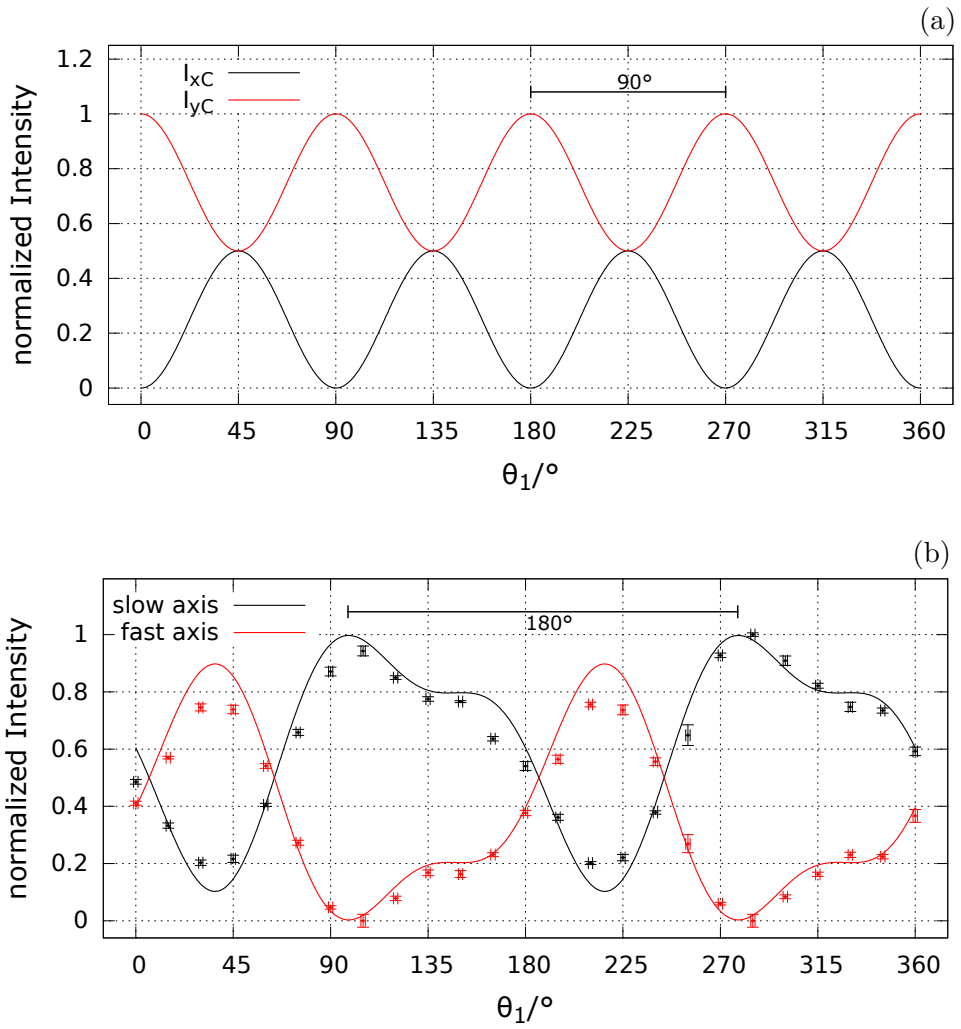

Fig. 3.6: (a) Simulation result illustrating the intensity in both cavity axes (I_{xC}, I_{yC}) for a rotation of the first waveplate. A special case occurs, if the axes of the cavity coordinate system are parallel to the ordinary and extraordinary axes of the second waveplate, resulting in 90° periodicity even for a $\lambda/4$-plate as first waveplate. $\theta_C = 0°$, $\theta_2 = 90°$.
(b) Fit to the splitting measurement in fig. 3.4 employing the simulation with a $\lambda/4$-plate as first waveplate. The fit is quite better than a sinusoidal fit. $\theta_C \approx 103°$, $\theta_2 \approx 47°$, $\phi_2 \approx 0.3\,\pi$, angle offset $\approx 14.4°$.

3.4 Further observations

While investigating polarization mode splitting, further observations have been made. These shall be mentioned here.

Asymmetry in the reflection signal

A fit of the reflection signals always reveals a slight deviation from a Lorentzian lineshape. One can observe an asymmetry as shown in fig. 3.7. The effect occurs in either cases, scan of the cavity length with increasing or with decreasing length. Comparing both cases, the effect seems to be "mirrored". An investigation on this behaviour is already timetabled in the research group.

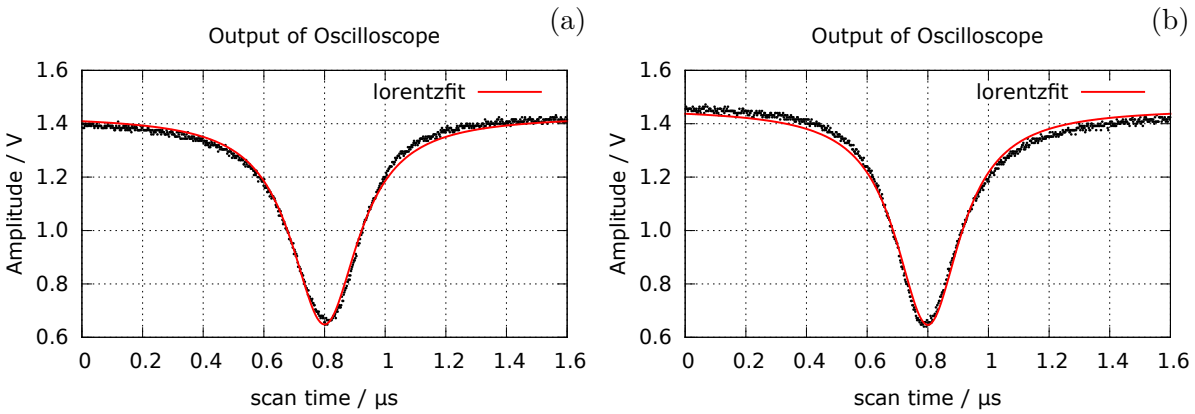

Fig. 3.7: Asymmetry in the reflection signal (with 850 nm) when the length of the cavity is scanned over the resonance with (a) decreasing and (b) increasing length.

Cavity ringing

Immediately after having scanned the length of a cavity over resonance, the intra-cavity light field starts to exponentially decay, characterized by the cavity-decay time. Considering the coating parameters at 780 nm for our fibers, the order of magnitude of this decay time is 10^{-8} s. If the cavity is scanned over its resonance faster than the decay time, a phenomenon called "cavity ringing" occurs. The output field features a modulation of its amplitude with increasing frequency. This can be understood by considering the interference between a laser field of constant frequency and an intra-cavity field with continuously shifted frequency due to the cavity scan [8]. Because its origin lies in the decay of the cavity field, the ringing is always found on the trailing edge of the peak independent of whether the cavity is scanned with increasing or decreasing length.

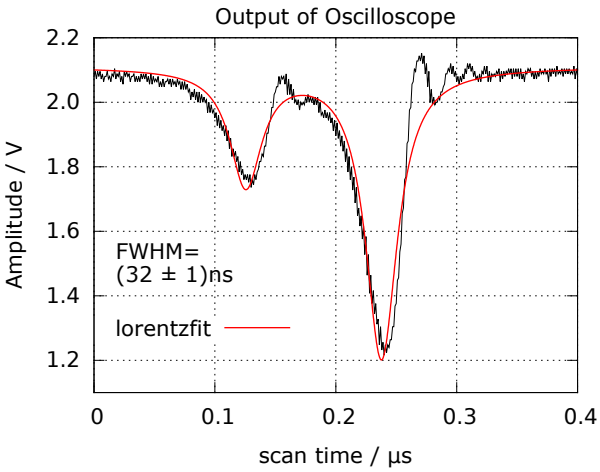

Fig. 3.8: Cavity ringing occurs for very fast scans over the resonance on time scales of 10^{-8} s. The output field features amplitude modulations with increasing frequency. Here, the full width at half maximum of the resonance is scanned within (32 ± 1) ns.

Minimization of polarization mode splitting

The polarization mode slitting inside fiber cavities causes two slightly different resonance frequencies. Consequently, the transmitted bandwidth becomes larger, which decreases the applicability of fiber cavities as optical filters. Polarization mode splitting can be minimized by a rotation of one fiber with respect to the other, so that the major ellipticity axis of one fiber mirror is opposed to the minor ellipticity axis of the other and vice versa. This "neutralizes" the ellipticity to a certain extent. Photos of a rotatable fiber mount can be found in appendix B.

4 Transmission efficiency

4.1 Theory

Two important figures of merit for optical filter cavities are a small bandwidth and high transmission on resonance. The first is determined by the finesse and the cavity length, the latter is characterized by the transmission efficiency, which is the ratio between incident and transmitted power. Unfortunately, in a cavity with losses L, these two are competing quantities. How to deal with this trade-off shall be analyzed in the following.

On its way through the setup light undergoes and is affected by several optical components and their efficiencies. For transmitted power we obtain:

$$\begin{aligned} P_{transmitted} &= P_{in} \cdot \eta_{path\_in} \cdot \epsilon_1\epsilon_2 \cdot \eta_{path\_out} \cdot T_{max} \\ T_{max} &= {}^{4T_1T_2}\!/_{(T_1+T_2+L_1+L_2)^2} \end{aligned} \tag{4.1}$$

In case of losses on the mirrors a maximum transmission $T_{max} < 1$ occurs (see section 2.1), which is inherent to the cavity mirror coatings at hand. $\eta_{path\_in,out}$ are the efficiencies of all optical components the laser light passes by, such as the fiber couplers or the splicing. What is left is the product of the mode-matching-efficiencies $\epsilon_1\epsilon_2$ of the fiber mirrors 1 and 2.

Mode-matching efficiency

A laser beam can mathematically be composed into Hermite-Gaussian modes, whereas the fundamental Gaussian-mode is of most importance for our experiments. It describes beams exiting single-mode fibers and thus entering the fiber-cavities. As pointed out in section 2.2, if the mode match between the fiber mode and the Gaussian cavity mode is large, the intra-cavity light field on resonance can be described to good approximation by a Gaussian beam as well. Considering the coupling of the fiber mode ψ_f to the cavity mode ψ_c, the power coupling or mode matching efficiency on mirror i is given by the squared absolute overlap integral [5],[9]:

$$\begin{aligned} \epsilon_i(\lambda, L, R_1, R_2, w_{f,i}, d) &= |\langle\psi_f \,|\, \psi_c\rangle|^2 = \frac{4}{\left(\frac{w_{f,i}}{w_{m,i}} + \frac{w_{m,i}}{w_{f,i}}\right)^2 + \left(\frac{\pi n w_f w_{m,i}}{\lambda R_i}\right)^2} \cdot \zeta \\ \zeta(\lambda, L, R_1, R_2, w_f, d) &= \exp(-({}^{d}\!/_{d_e(\lambda,L,R_1,R_2,w_{f,i})})^2) \end{aligned} \tag{4.2}$$

Here, $R_i, w_{m,i}, w_{f,i}, L$ denote radius of curvature of mirror i, cavity mode field radius on mirror i, fiber mode radius of fiber i and length of cavity, respectively. Mind that ellipticity of the mirror surfaces is neglected in this formula. R_1 and R_2 refer to the two different fiber mirrors and not to the two ellipticity axes of one and the same mirror as in chapter 2 and 3. The second part of the denominator results from the lensing effects and wavefront curvature, since the beam wavefront, after having passed through the mirror, has radius of curvature $R_{beam} = \frac{R_i}{n-1}$ with n the refraction index of the fiber core. Moreover, a decentration d is taken into account which exponentially damps the mode matching efficiency. The same is valid for angular misalignment of one fiber with respect to the other. For a full expression of d_e and additional information about angular misalignment which is neglected here, see [9].

4.2 Optimizing transmission efficiency

Achieving a high transmission efficiency can be fulfilled by two independent possibilities: maximization of the product $\epsilon_1\epsilon_2$, which depends on the alignment and the geometry of the fiber mirrors, and maximization of the maximal achievable transmission T_{max}, which depends on the mirror coatings. In the following analysis a cavity with a singlemode input and a multimode output fiber (with coating parameters presented in tab. 2.1) is assumed. Because the output fiber is a multimode fiber with large numerical aperture, it gathers almost all the light exiting the cavity and its decentration has no effect so that we can assume $\epsilon_2 = 1$.

Maximization of mode matching efficiency $\epsilon_1\epsilon_2$

The geometry of the cavity is a very important factor to obtain large mode matching. As it can bee seen in equation (4.2), the mode match ϵ_1 between the SM-fiber mode and the cavity mode increases to a maximum if the SM-fiber mode field radius $w_{f,SM} = (2.4 \pm 0.1)\,\mu m$ is identical to the cavity mode field radius $w_{m,1}$ on the mirror of the singlemode fiber. The multimode fiber is not that sensitive on this condition as it gathers the intra-cavity light anyway ($\epsilon_2 = 1$), considering its large numerical aperture and the small divergence of the cavity beams. Consequently, in order to achieve high mode matching efficiency, the cavity geometry has to be chosen such that the Gaussian beam inside the cavity is sharply focused on the singlemode mirror surface and attains a beam radius of $w_{m,1} \approx w_{f,SM}$!

This can be fulfilled by taking care of the curvature of the multimode fiber mirror. The larger its curvature, the sharper will the beam be focused onto the singlemode fiber mirror, as illustrated in fig. 4.1. With $R_2 = 50\,\mu m$, the radius of the cavity beam on the SM-mirror obtains 2 µm to 2.5 µm for cavity lengths between 5 µm to 45 µm. This definitely agrees with the radii condition and results in an almost 100 % mode matching for this range of mirror distances. Furthermore, in order to minimize lensing effects, a flat singlemode fiber ($R_1 = \infty$) should be chosen. The resulting mode matching is depicted in fig. 4.2, solid lines.

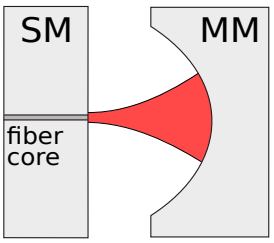

Fig. 4.1: Optimum geometry for a SM-MM combination.

In order to obtain a very high coupling for a cavity consisting of two singlemode fibers, the beam radii on *both* mirrors have to agree with the radii condition. Thus, the probable optimal geometry is a symmetric cavity ($R_1 = R_2$). In this constellation the beam radii on both mirrors are identical. This constellation has not been investigated further.

Avoiding decentration and misalignment is another keyword since both exponentially damp transmission. Although decentration is due to production issues of the fiber mirrors and cannot be corrected afterwards, it is possible to minimize its effects by aligning the fibers in a way illustrated in fig. 4.3. Due to a tilt of the fibers, the effective decentration $d_c - d_f$ is smaller than the inherent decentration d_f. However, this introduces angular misalignment which also causes a decrease in mode matching. So, a compromise between both has to be found. Furthermore, one has to balance the degree of freedom of rotating the fibers with respect to each other between minimizing decentration effects and minimizing polarization mode

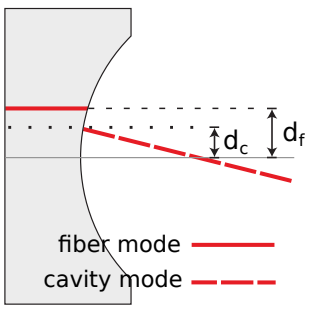

Fig. 4.3: Minimizing decentration effects by the alignment.

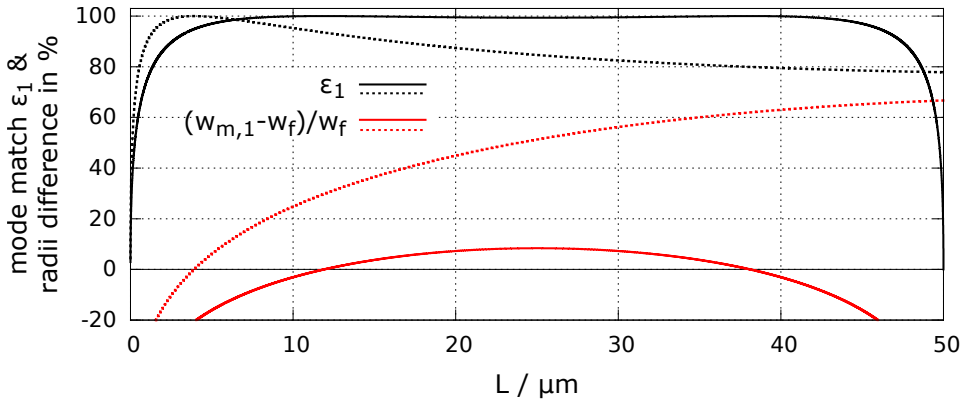

Fig. 4.2: The mode matching efficiency is very sensitive on the condition $w_{m,1} \approx w_{f,SM}$. A small radius of curvature $R_2 = 50\,\mu\text{m}$ of the multimode mirror sharply focuses the cavity beam onto the singlemode fiber, so that the condition is approximately satisfied. By employing a flat singlemode fiber, lensing effects vanish. The result (solid lines) is $\epsilon_1 \approx 100\,\%$ for a long range of cavity length. The abrupt drop at $L = 50\,\mu\text{m}$ is due to geometric instability. With $R_2 = 120\,\mu\text{m}$ (dashed lines), the mode match decreases about 22 % due to larger deviations of the radii.

splitting. All in all, that makes three quantities forming a trade-off. That is why finding a more reliable way of fiber-mirror fabrication with lower decentrations is the best option here.

Considering a Gaussian mode with its infinitely wide power distribution inside a cavity with finite mirror-diameter D_i, a "clipping" loss has to be taken into account[4]. Upon every reflection on mirror i the clipping loss reads [5]

$$L_{cl,i} = \exp(-2(D_i/2w_{m,i})^2). \tag{4.3}$$

These clipping losses effect finesse and T_{max} which become functions of the cavity length and consequently drop at large fiber distances. As an example, for a cavity with $R_1 = R_2 = 180\,\mu\text{m}$ (which is a typical value of our fibers) and no decentration on the singlemode fiber mirror, the finesse and T_{max} drop around a cavity length of 90 µm as depicted in fig. 4.4a. The maximum transmission efficiency can be found at cavity lengths between 3 µm to 5 µm for the parameter ranges of our fibers, because here the cavity mode field radius $w_{m,1}$ on the mirror of the SM fiber is identical to the SM-fiber mode field radius $w_{f,SM} = (2.4 \pm 0.1)\,\mu\text{m}$ (illustrated by the blue dashed line) which results in almost 100 % mode coupling efficiency ϵ_1. The remaining mismatch is due to the mirror curvature.

Maximization of T_{max}

On the other hand, taking care of the dielectric coatings on the fiber tips is is also required to reach the highest possible transmission of a Fabry-Perot filter cavity. But as mentioned before, as long as the coatings have losses, transmission and finesse are competing quantities. While the first requires a high coating transmission, the latter requires low coating transmission. This can be seen in fig. 4.4b. If the coating losses are really low, for example $L = 1\,\text{ppm}$ (dashed lines), the transmitted power is almost

[4]The mirror-diameter D can be found via a Gauss-fit of the mirror surface, see section 2.3.

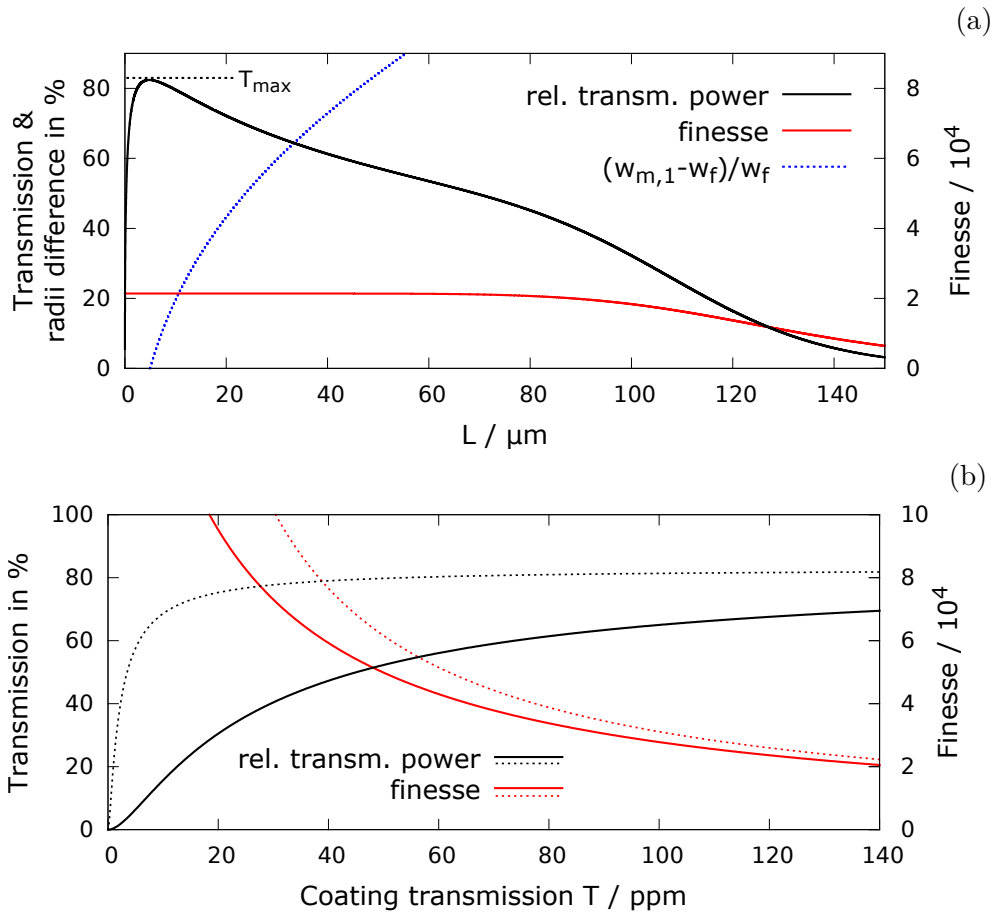

Fig. 4.4: (a) Transmission and finesse vs. cavity length for a symmetric singlemode-multimode cavity with $R_1 = R_2 = 180\,\mu\text{m}$, no decentration and light at 850 nm wavelength. The drop at 90 µm is due to clipping losses. The maximum transmission can be found around 5 µm because here $w_{m,1} = w_{f,SM}$. (b) Transmission and finesse vs. transmission of coating for the same cavity as in (a) with laser light at 850 nm and at a typical cavity length of 25 µm. For low losses $L = 1\,\text{ppm}$ (dashed lines) one can obtain both, high finesse and high transmission efficiency. For larger losses $L = 13\,\text{ppm}$ (solid lines) it is rather a trade-off. In both cases no decentration is assumed.

constant for fiber mirrors with coating transmissions above 10 ppm. Thus, one can obtain high transmission efficiency around 75 % and also large values of finesse above 100 000 simultaneously. However, using the coating properties of our fibers with losses around 13 ppm (solid lines), one has to decide between large transmission *or* large extinction, large free spectral range and narrow bandwidth.

All things considered, in order to obtain a singlemode-multimode filter cavity with large transmission on resonance, the geometry of the cavity is of uttermost importance. A flat singemode fiber mirror and a strongly curved multimode fiber mirror will lead to an almost perfect mode matching. The losses in the mirror coatings cause a trade-off between large finesse and large power transmission on resonance. The choice between these two quantities has to be made with respect to the specific application for which the cavity shall be employed. In the case of decentration on the singlemode fiber, its effects can be decreased by angular misalignment. However, it is always better to choose a fiber with less decentration.

4.3 Measurements

In an experiment with the SM-MM cavity the theoretical model above should be verified. Therefore, the transmitted power has been recorded for different cavity lengths with the setup in fig. 4.5a. By analysing microscope camera photos, the fiber mirror distances have been measured; a calibration from pixels to metres is possible because the cladding diameter of the SM fiber is well-known. The amplitude of the transmission peak, which is recorded with a photodiode and an oscilloscope, yields the amount of transmitted light on resonance. For every new set length the fibers have been aligned again so that the transmission peak on the oscilloscope increased to its maximum. This procedure minimizes misalignment effects which occur when the fibers are moved apart or together and results in the best trade-off between angular misalignment and effective decentration.

The measurement result is shown in fig. 4.5b. Since the effective decentration and the angular misalignment are unknown, the theoretical prediction (solid line) has been calculated assuming no angular misalignment and thus full decentration (which is 1.824 µm for the SM-fiber). This means, that the theoretical prediction represents a lower limit for the transmission to be expected. Since the fibers have been aligned for maximum transmission peaks (that means for the optimum trade-off between angular misalignment and effective decentration) at every length, all data points should be located above the solid line.

However, a large discrepancy between experimental results and theory can be observed. Measuring a transmission between 26 % to 20 % for typical cavity lengths up to 30 µm, the SM-MM-cavity transmits even less light than the theoretical lower limit predicts. This attenuation could be due η_{path}, that means the effect of the optical components which the laser light passes by. One possible source is the splicing of the SM-fiber, which could be defect and reflect a lot of light, leading to a decrease in transmission efficiency. A measurement of the mirror coating transmission of the SM fiber yields (134 ± 4) ppm for light at 850 nm, which coincides with the coating transmission of our other mirror fibers. This implies that the splicing does not have a dominant influence on the transmitted power. The beamsplitter can be excluded as well, since its non-perfect 50/50 splitting into the channels one and two has been taken into consideration in the experiment.

In order to make the SM-MM-cavity usable as an optical filter with high transmission on resonance, a more detailed examination on the contribution of the optical components which probably damp the transmission efficiency should be scheduled. For example, to be really sure about the effects of the splicing, one could measure the transmission of the fiber directly after and in front of the splicing. However, this is not possible in a non-destructive way. Due to time issues, this idea could not be checked during the bachelor project.

(a)

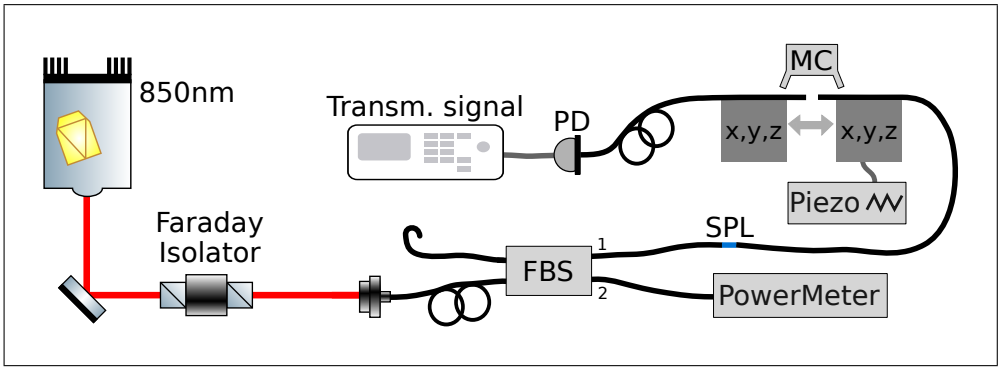

(b)

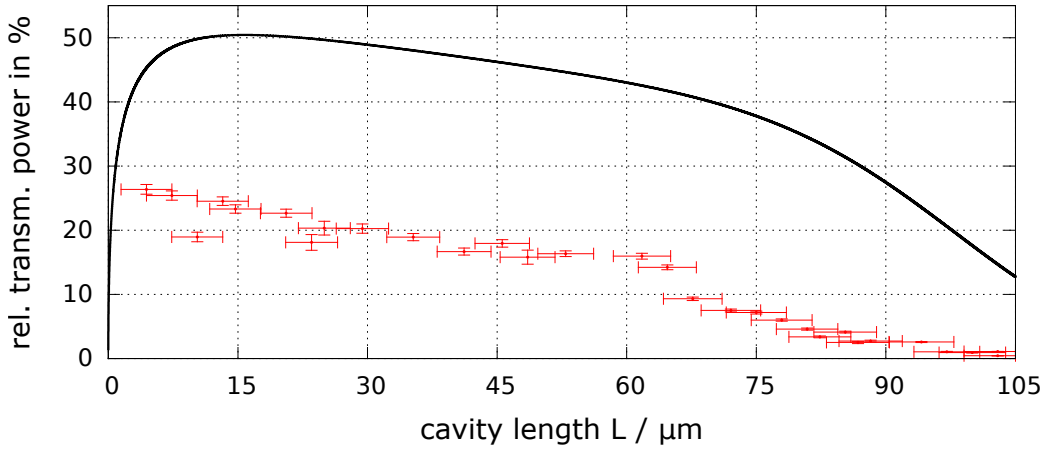

Fig. 4.5: (a) Setup of the transmission measurement with 850 nm and a fiber beamsplitter (FBS). The transmission signal is recorded with an oscilloscope, the cavity length has been estimated from microscope camera (MC) images. SPL=splicing. (b) The transmission measurement shows a large discrepancy between the recorded data and the theory. The solid line represents a lower bound of the transmission to be expected. Obviously, some components in the setup attenuate a lot of light. Errors on the cavity length are dominated by the resolution of the microscope camera.

5 Conclusion & Outlook

The topic of this thesis was the examination of two important characteristics of fiber-based Fabry-Perot resonators, of which the first one was polarization mode splitting. Polarization mode splitting inside a fiber cavity is due to ellipticity of the fiber mirrors. It is the reason for the appearance of two slightly different resonance frequencies. In the SM-MM cavity the displacement of the polarization eigenmodes was around 75 MHz, which provided a good opportunity to investigate the behaviour of the mode splitting in more detail. A simulation was employed to calculate the population of the two polarization modes as a function of the waveplate rotation. The effect of the fiber on incident polarization states was simulated by assuming it acts as an arbitrary waveplate. The measurements verified the results: By the rotation of a $\lambda/2$ retardation waveplate, the polarization modes are populated and depopulated with a periodicity of 90°. Using a $\lambda/4$-plate instead, the periodicity is 180° and not longer sinusoidal, despite some special cases. In terms of its effects on polarization states, it seems suitable to approximate a singlemode fiber as an arbitrary waveplate. Moreover, the earlier non-understood measurements in the research group could be clarified. They resulted from the use of an incorrect waveplate.

Large transmission on resonance is an essential figure of merit of a fiber-based filter cavity. The mode match between the fiber mode and the Gaussian cavity mode obtains a maximum, if the beam radius of the cavity mode on the mirror surface is identical to the fiber mode radius. It has been shown for a cavity consisting of a singlemode input and a multimode output fiber, that a flat SM- and a strongly curved MM-fiber satisfy this condition, which results in an almost perfect mode matching for a long range of cavity length. Furthermore, it has been outlined that with the coating losses of our fibers the finesse and the maximal achievable transmission form a trade-off. Experimental verification however was not successful. It seems that optical components in the setup attenuate a lot of light.

So far, the SM-MM cavity features the properties presented in tab. 5.1. Despite the quite small transmission, especially the combination of narrow bandwidth and large free spectral range makes it outstanding compared to usual commercial optical filters. For example, an optical filter based on a Bragg grating of the company OptiGrate[5] provides transmission bandwidths of several 10 GHz, which is 3 orders of magnitude larger than the bandwidth of the SM-MM cavity. A macroscopic Fabry-Perot resonator produced by the company Quantaser[6] features a much smaller bandwidth of 80 MHz, which is comparable to the bandwidth of the SM-MM cavity, but the free spectral range is only around 20 GHz.

In order to develop fiber Fabry-Perot cavities into practical filter devices, it will be necessary to precisely stabilize their resonance frequencies. This could be realized by glueing the mirror fibers into an optical glass ferrule. Another important figure of merit is thereby introduced: Temperature stability. An analysis and optimization of this quantity would be an exciting project in future.

[5] BragGrate™ - Bandpass Filter. OptiGrate, Oviedo, FL. `http://www.optigrate.com`

[6] FPE002. Quantaser, Taiwan. `http://www.quantaser.com`

	850 nm	780 nm
Finesse $\mathscr{F}$	$24\,300 \pm 300$	$189\,000 \pm 8000$
FSR / THz	5.0 ± 0.5	5.0 ± 0.5
Linewidth FWHM / MHz	183 ± 4	23 ± 1
Mode splitting / linewidths	not observed	3.22 ± 0.10
Transmission / %	20 ± 1	not measured
Extinction γ / dB	41.9 ± 0.1	50.8 ± 0.2

Tab. 5.1: Summary of the measured finesse, linewidth, splitting and transmission efficiency of the SM-MM cavity for a cavity length of $(30 \pm 3)\,\mu$m. FSR and extinction are calculated via eqs. (2.4) and (2.14), respectively.

Appendix

A Accuracy of the finesse measurements

In this thesis, finesse has been measured with the setup depicted in fig. 3.1. The input fiber was situated on a three-dimension stage equipped with a piezo crystal. By plugging in a triangle voltage, the piezo moves the fiber towards and backwards so that the cavity length is scanned over two adjacent orders of resonance. Thus, one can simultaneously measure the free spectral range and the linewidth of the transmission and reflection peaks in units of time. The ratio of both yields the finesse and deviations yield the error.

The fiber has to be moved by a distance of $\lambda/2 \approx 400\,$nm to shift the cavity from one order of resonance to the next order. For the calculation of the cavity finesse the piezo movement was assumed to be perfectly linear over the entire scan range. As I learned later, the piezo movement cannot assumed to be linear in this range. That introduces a systematic error on the finesse values presented in section 2.5. Due to time issues, the error due to non-linearities in the cavity scan could not be investigated.

A more accurate and precise way of measuring the finesse of a cavity is the following: The cavity length will only be scanned over one single transmission peak so that trouble with the piezo properties will be prevented. One employs two lasers emitting light into the cavity and sets the difference of their frequencies to exactly one free spectral range of the cavity. This can be fulfilled by setting them at first to the almost identical frequency and observing both transmission peaks on the oscilloscope. Then the frequency of one laser is altered until it is again resonant with the cavity. This manifests in a reappearance of the second resonance peak on the oscilloscope. When these peaks completely overlap, one can measure the frequency difference of the lasers with a wavemeter and thus obtain a value for the free spectral range. The absolute linewidth of the cavity would still be measured by making use of calibrated sidebands as described in section 3.2. This kind of measurement could be utilized for future finesse measurements.

B Photos of the alignment stages and opposed fibers

The following photos show the setup that was used to align the two fiber mirrors opposing each other. Each photo is a zoom-in of its prior photo.

In fig. B.1 the three-dimension alignment stages can be seen, as well as the cables connecting the piezo of the right stage with a frequency generator. The fibers are situated in V-grooves which are depicted in fig. B.2. The singlemode fiber is furthermore clamped in a rotatable mount so that the fibers can be rotated with respect to each other. This degree of freedom is usually utilized to decrease mode splitting by opposing the major ellipticity axis of one fiber mirror to the minor ellipticity axis of the other and vice versa.

The same situation as in fig. B.2 is photographed with the microscope camera, shown in fig. B.3. The distance of the fiber tips is approximately $(34 \pm 3)\,\mu\text{m}$. This can be calibrated because the cladding diameter of the singlemode fiber is well-known.

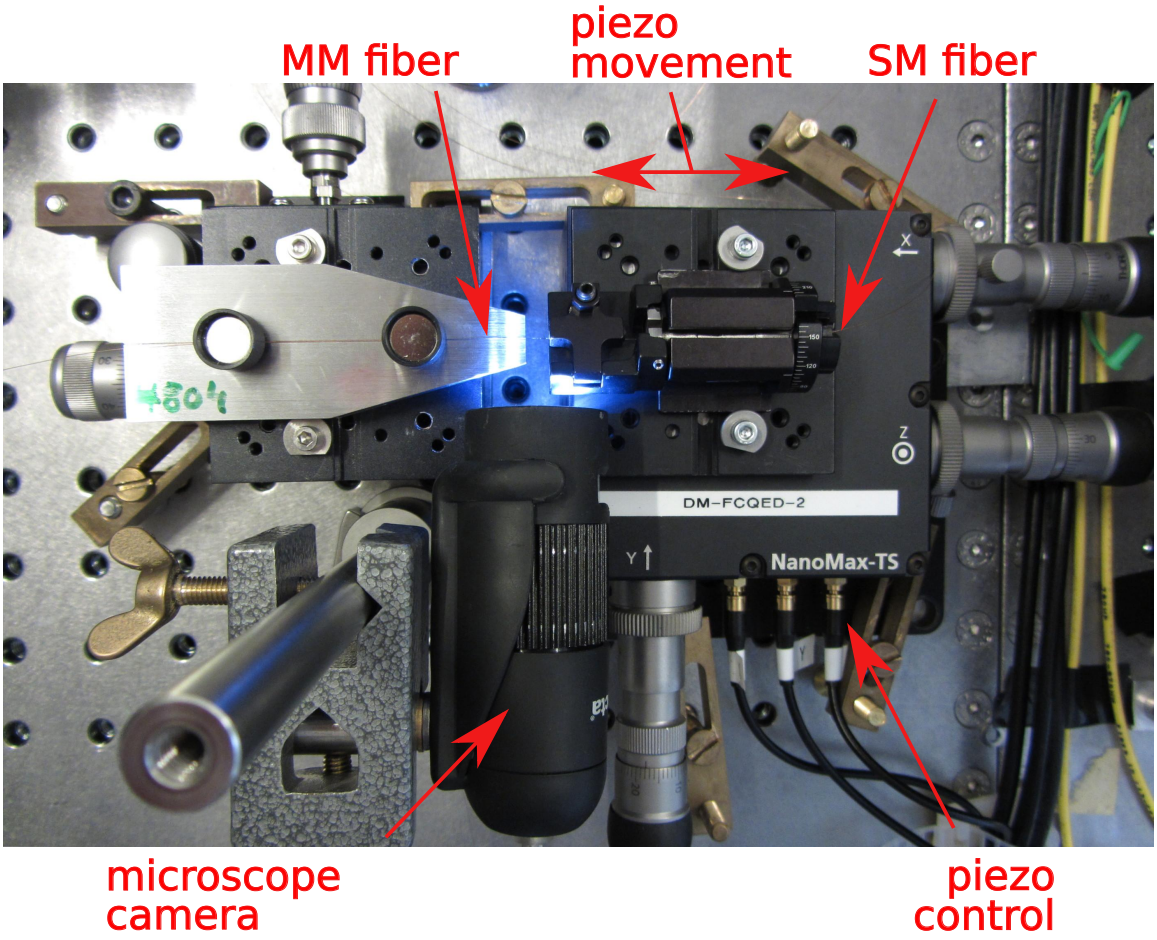

Fig. B.1: Photo of the three-dimension alignment stages.

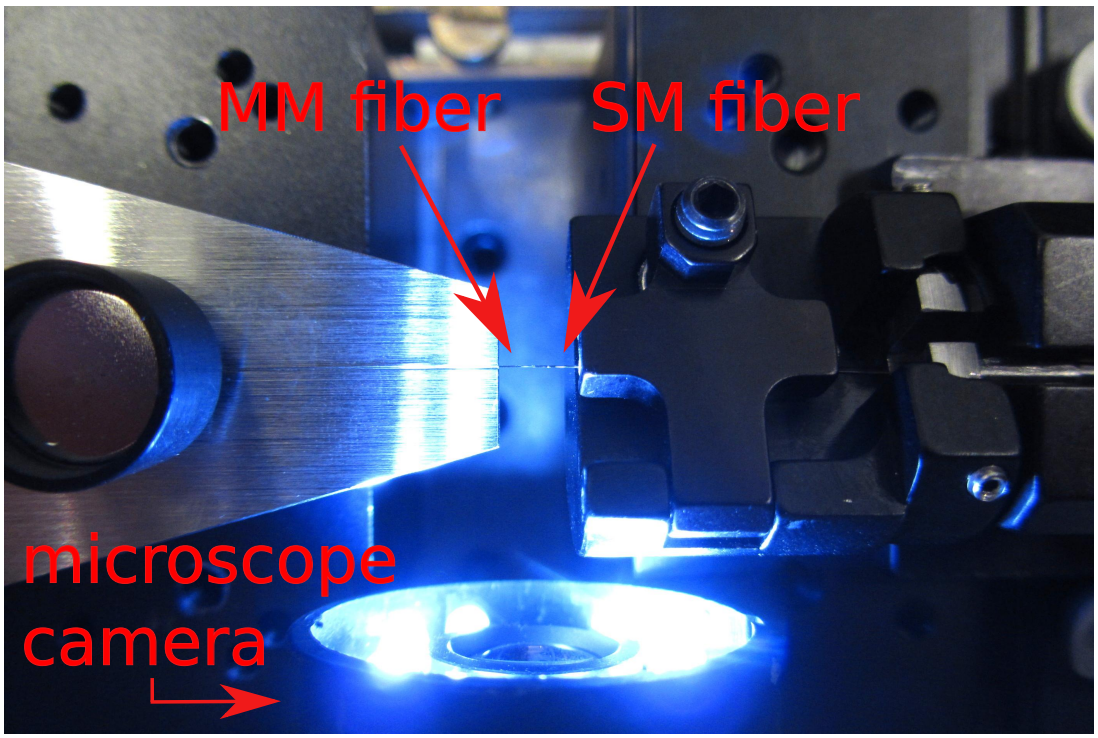

Fig. B.2: Photo of the opposed fibers of the SM-MM cavity. The photo is a zoom-in of fig. B.1.

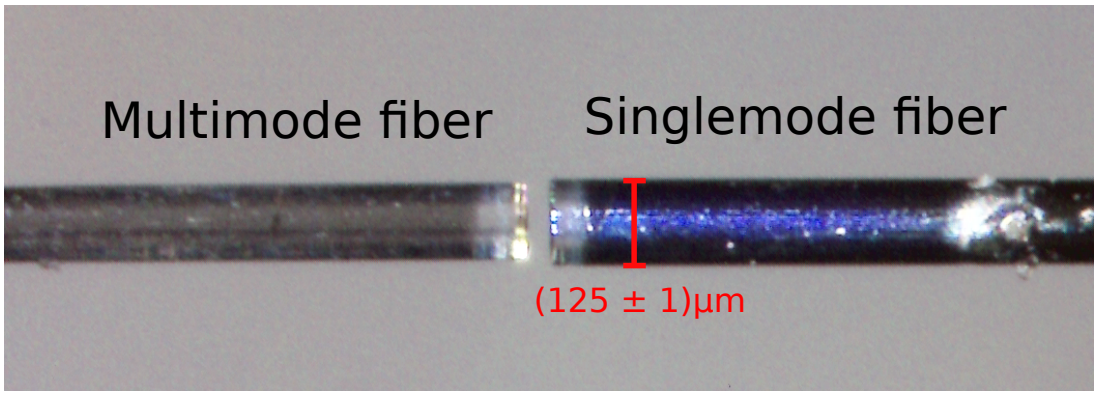

Fig. B.3: Microscope camera photo of the opposed fibers in fig. B.2. The cavity length is $(34 \pm 3)\,\mu\text{m}$. The background is white because a white paper has been situated there when taking the photo.

Acknowledgements

I would like to thank the whole research group of Professor Meschede for providing a friendly and kind atmosphere. The members of the fiber cavity group who patiently answered my questions and helped me deserve special thanks. I want to thank Prof. Dr. Meschede for providing me the opportunity to work on this interesting project and moreover to integrate me into the research group's daily life. This insight into how current research "takes place" was really interesting and gave me a clue of how diverse the work in experimental physics is.

References

[1] G. Rempe et al. “Frequency splitting of polarization eigenmodes in microscopic Fabry-Perot-cavity”. In: *New Journal of Physics* 17.1 (2015), p. 013053.

[2] C. Hoyer. *Aufbau eines Resonators hoher Finesse zur Linienbreitenmessung*. BA thesis. Technische Universität Darmstadt. 2013.

[3] B.E.A. Saleh and M.C. Teich. *Fundamentals of Photonics*. John Wiley & Sons, Inc., 1991.

[4] ”Gaussian beam with german description-1” by Aleph - Own work. Licensed under CC BY-SA 2.5 via Wikimedia Commons.

[5] D. Hunger et al. “A fiber Fabry-Perot cavity with high finesse”. In: *New Journal of Physics* 12.6 (June 2010), p. 065038.

[6] D. Hunger et al. “Laser micro-fabrication of concave, low-roughness features in silica”. In: *AIP Advances* 2.1 (2012), p. 012119.

[7] D. Goldstein. *Polarized Light*. 2nd ed. Marcel Dekker, Inc., 2003.

[8] I. Dotsenko. “Single atoms on demand for cavity QED experiments”. PhD thesis. University of Bonn, 2007.

[9] W. B. Joyce and B.C DeLoach. “Alignment of Gaussian beams”. In: *Appl. Opt.* 23.23 (Dec. 1984), pp. 4187–4196.

List of Figures

Ich versichere, dass ich diese Arbeit selbständig verfasst und keine anderen als die angegebenen Quellen und Hilfsmittel benutzt sowie die Zitate kenntlich gemacht habe.

Bonn, den _____ Unterschrift _____